Resonant Optical Transmission through Topologically Continuous Films

Bin Ai,[†] Ye Yu,[†] Helmuth Möhwald,[‡] Limin Wang,[†] and Gang Zhang[†,*]

[†]State Key Lab of Supramolecular Structure and Materials, College of Chemistry, Jilin University, Changchun 130012, People's Republic of China, and
[‡]Max Planck Institute of Colloids and Interfaces, D-14424 Potsdam, Germany

ABSTRACT A continuous thick (≥100 nm) Ag film is generally optically nontransparent, but here we show that *via* a dedicated structuring it can be made transparent. The enhanced optical transmission is realized by preparing metal films with a periodic array of hollow nanocones *via* an inexpensive and versatile colloidal lithography technique. These topologically continuous films possess the structural feature of sharp top tips and bottom nanoholes, leading to an effective resonance mode of coupling between the surface plasmons around the holes and cone tips. This introduces a resonant optical transmission that is much affected by the thickness and height of the hollow nanocones. Moreover, the topologically continuous films are highly sensitive to the surrounding environment, indicating great potential for plasmonic sensors. The experimental results are in good agreement with numerical simulations. On the basis of the hollow element and enhanced optical performance, hollow nanocone array films can be used as photosensitive microreactors, isolated cell culture bases, *etc.* This provides a combination of high optical sensitivity and chemistry in microcavities.

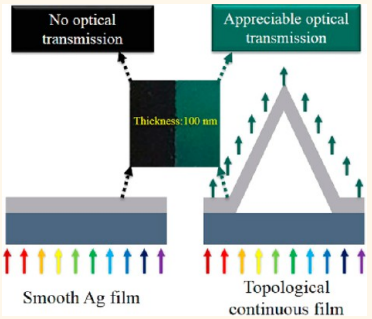

KEYWORDS: surface plasmon resonance · optical transmission · hollow nanocone · colloidal lithography

It is well known that light can only be transmitted through thin films or perforated films, while being blocked by continuous (without holes) thick metal films. However, this paper experimentally and theoretically introduces a phenomenon where light easily passes through an optically thick continuous film with topological structure. In recent years, the field of light tunneling through continuous metal films has attracted much attention. Apart from its fundamental interest, if this optical effect is quantitatively established, it may have great potential for the next generation of photonic devices and sensors. Furthermore continuous thick films with strong optical transmission can be applied in cases needing airtight/isolated environments, which are difficult to realize for perforated films and in cases needing stronger mechanical strength than that of thin films.

Because of wide application prospects and unique advantages, large efforts have been made to achieve strong optical transmission through continuous thick metal films. It has been found that when light illuminates metal films, surface plasmons (SPs)—collective excitations of surface electrons induced by light—are excited at the metal/dielectric interface.[1−4] A planar structure consisting of a thick metal film sandwiched between two semi-infinite dielectrics supports two independent surface plasmon resonances (SPRs) at both sides of the metal film, resulting in low optical transmission, which is difficult to actually use in practical applications. Further research on the resonant optical transmission through thin metallic films with and without holes proved that the presence of holes is not necessary for the extraordinary optical transmission.[5] Recently, thick metal films with ridge gratings have been theoretically studied, indicating the possibility to obtain higher transmission by more effective SP excitation.[6,7] Other than these impressive works, further research (especially experimental studies) in this still young yet very promising field of optical transmission through continuous thick films is still scarce, but novel types of continuous thick metal films with higher transmission performances are highly demanded.

* Address correspondence to gang@jlu.edu.cn.

Received for review November 9, 2013 and accepted January 7, 2014.

Published online January 07, 2014
10.1021/nn4058177

Moreover, the generation and development of desirable nanostructures are mainly due to advances in nanofabrication methodologies. While scanning beam techniques such as electron beam (EBL)[8] and focused ion beam lithography (FIB)[9] are capable of precise control over size, shape, and spacing of metallic nanostructures, more recent research has focused on unconventional lithographic techniques that are capable of patterning large areas (in macroscopic dimensions of dozens of square centimeters or more) in parallel at low cost. Colloidal lithography has been widely exploited in the fabrication of surface plasmonic structures, possessing advantages of lower cost, higher throughput, greater flexibility, and easier implementation. By using two-dimensional arrays of colloidal spheres as templates, metal crescents, discs, holes, and split-ring resonators have been prepared by the various metal evaporation processes and reactive-ion etching procedures.[10−14]

Here, on the basis of our previous work on developing colloidal lithography,[15−17] we have developed a method to prepare a structured silver film with a hollow nanocone array. The topologically continuous film is demonstrated to show greatly enhanced optical transmission compared to a flat film with the same thickness. The hollow nanocones possess sharp top tips and bottom nanoholes, which are both prominent places where strong SPRs can be excited.[18−22] Due to the contributions of SP energy from these two types of structures, the SP field of hollow nanocones is not only greatly enhanced but also redistributed inside the hollow core (air) outside the dielectric substrate, resulting in a new kind of resonant optical transmission. Furthermore, the effect of structural parameters on the spectra and sensing performances is investigated, showing precise control over the spectra and great potential for plasmonic sensors. The experimental results are in good agreement with numerical simulations. Hollow nanocone array films (HNAFs) fabricated by our efficient fabrication process are believed to lead to a new class of optical applications and also can be used as components in advanced photonic circuits and as detecting substrates in medical diagnostics.

RESULTS AND DISCUSSION

Fabrication of Hollow Nanocone Array Films. Films with highly ordered hollow nanocone arrays were fabricated based on a well-developed colloid lithography approach.[17] Figure 1 outlines the fabrication process and shows the schematic of a single hollow nanocone. First, a photoresin film with a thickness of ~2 μm was spin-coated onto glass substrates. Then a hexagonally close-packed colloidal monolayer was assembled on the substrate by the interface method.[23] Then reactive ion etching (RIE) was carried out for 4 min to completely etch away the microspheres and construct the photoresin film into a periodic cone array. Next, 100 nm

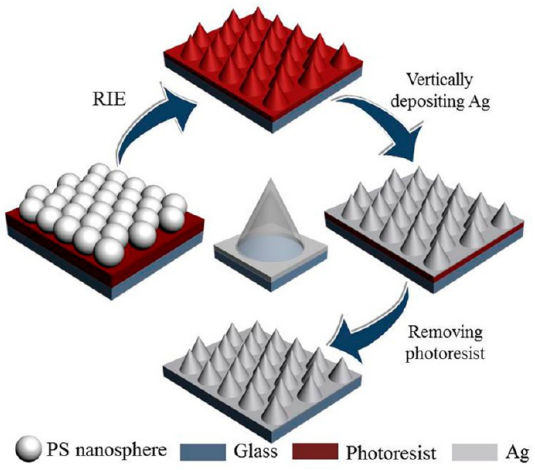

Figure 1. Outline of the process for fabricating hollow nanocone array films. The central schematic shows a transparent hollow nanocone to stress the relevance of the central structural element.

Ag was vertically deposited onto the substrate in a thermal evaporator. Finally the samples were immersed slowly into ethanol and laid flat on the bottom for one hour. In case there still remained photoresin film between the Ag film and the substrate, this could be dissolved completely by ethanol, leaving the hollow nanocone array supported on the glass substrate at its original site. The period, height, and thickness can be well controlled by the diameter of PS spheres, etching parameters, and deposition duration (rate), respectively, in the fabrication process. The method is versatile, inexpensive, and capable of patterning large areas in parallel at low cost and can be applied with only little sophisticated equipment, yet with good control of the main structural parameters.

When RIE processes with increasing durations are carried out, the PS microsphere mask becomes smaller and the photoresin film is etched into an array of truncated cones with increasing heights (Supporting Information Figure S1). If the RIE duration is increased to 4 min, the PS mask is removed completely, resulting in a periodic array of hollow nanocones with a height of 600 nm and diameter of 400 nm. Figure 2a shows that the hollow nanocone arrays are fabricated uniformly over a large area of hundreds of square micrometers. Figure 2b and c provide a view at 45° of a highly magnified scanning electron microscopy (SEM) image and a 3D atomic force microscope (AFM) image of the HNAF, which present well-defined cone shapes with sharp tips and prove that the film is continuous and has no pinholes over a large area. Figure 2d shows a SEM image of the reverse side of the HNAF, where the red arrow indicates the hollow-core construction. Cross-sectional views of photoresin cones and Ag hollow cones are shown in Figure 2e and f, respectively. It can be seen in Figure 2f that the thickness of the deposited Ag is 100−110 nm. Furthermore, the shapes of the

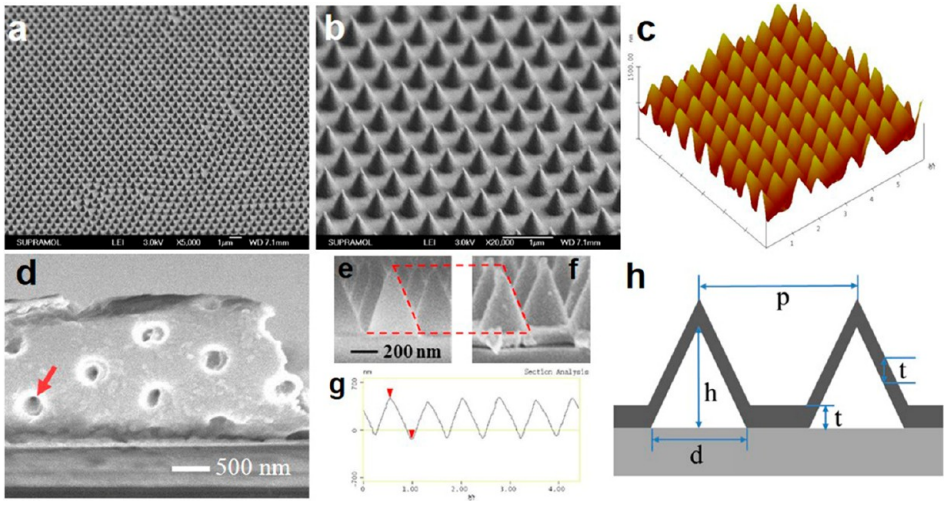

Figure 2. Typical SEM images of (a) a hollow nanocone array for a large area and (b) the magnified HNAF. The SEM images (a, b) are taken from a 45° tilting view. (c) 3D AFM images of the hollow nanocone array. (d) SEM image of the reverse side of the HNAF. The red arrow in (d) indicates the hollow-core construction,; (e) and (f) are cross-sectional views of photoresin cones and Ag hollow cones. The red dotted lines indicate that the shape does not change by the deposition process. (g) AFM profile of the hollow nanocone array to show the uniform height. (h) Drawing of the hollow nanocone array and main structural parameters of height (h = 600 nm), diameter (d = 400 nm), period (p = 700 nm), and thickness (t = 100 nm).

photoresin cones and Ag hollow cones are exactly the same, proving that Ag vapor is uniformly deposited on the cones, and the thickness (t in Figure 2h) in the vertical direction is everywhere 100−110 nm (for convenience, the thickness is regarded as 100 nm). The surface characterization from AFM (Figure 2g) shows that the height (h) is 600 nm and uniform. A drawing of the hollow nanocone array as well as main structural parameters of height (h), diameter (d), period (p), and thickness (t) are shown in Figure 2h to make the key structural elements clear. According to these structural characteristics, HNAF represents a topologically continuous Ag film, furthermore possessing the features of sharp top tips and bottom nanoholes.

By further prolonging the RIE duration, hollow nanocones with decreasing heights and diameters can be fabricated, which are shown in Figure 3. The height changes significantly from 600 nm to 200 nm, and the diameter changes much more slightly from 400 nm to 280 nm. All samples retain well-defined cone shapes with excellent uniformity. Besides, small gaps can be observed between the Ag films and the substrates, which results from the fact that the film deposits onto the substrate not over the entire area, because there is a photoresin film between the Ag film and the substrate before the dissolution procedure. For the following investigation on sensing performance, these gaps may allow species to be detected entering into the hollow core due to capillary forces. Although with gaps, the capillary force between Ag film and substrate also stabilizes the whole structure to enable the following measurements for dozens of times.

Resonant Optical Performance of Hollow Nanocone Array Film. Figure 4a shows typical measured and simulated zero-order transmission spectra for the HNAF and a

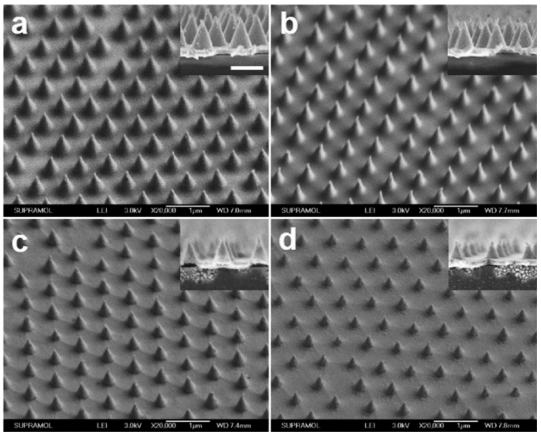

Figure 3. SEM images (45° tilting views) of hollow nanocones with a height/diameter of (a) 500/350 nm, (b) 400/320 nm, (c) 300/300 nm, and (d) 200/280 nm. The insets show the cross-sectional SEM images of the corresponding samples. The scale bar in the inset corresponds to 500 nm and applies to all the inset images.

spectrum of a smooth Ag film with the same average thickness (100 nm). The smooth and topologically uniform films are illuminated vertically, and the integral light propagation distances through these two films are both 100 nm (indicated by t in Figure 2h). However, the spectra show a number of distinct features based on the two films with different surface conditions. At a wavelength of ~330 nm a narrow bulk silver plasmon peak is observed that disappears as the film becomes thicker. No other peaks are observed for the spectrum of the Ag film (black curve), and the transmission is nearly zero at longer wavelengths. According to previous theoretical calculations, light cannot pass through a flat silver film with a thickness of 100 nm.[24] But in Figure 4a, a sharp optical

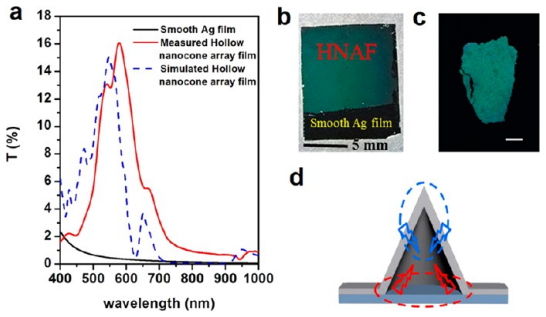

Figure 4. (a) Measured (red curve) and simulated (blue dash curve) transmission spectra of a HNAF and a 100 nm Ag film with the same thickness (black curve). (b) Optical image of an HNAF sample with a small part of a smooth Ag film at the bottom. (c) Optical image of an HNAF island surrounded by a 100 nm smooth Ag film. The scale bar corresponds to 10 μm. (d) Description of one single unit of the hollow nanocone array and the predicted mechanism generating the greatly enhanced optical transmission.

transmission peak at 577 nm is observed in the spectrum of the HNAF (red curve), proving a greatly enhanced optical transmission. The resonant transmission of the main transmission peak can be enhanced up to 40 times compared with that of the smooth film, although the two films have the same light propagation lengths. Moreover, the measured profile (red curve) is in good overall quantitative agreement with the simulated profile (blue curve). The remaining discrepancy can be attributed to extra energy losses in the metal due to increased surface scattering due to the rough Ag surface and the inhomogeneity of the inter-nanocone separation. The good agreement also indicates that inevitable defects based on the colloidal lithography (CL) technique have little influence on the optical performance. When a sample possessing both a smooth Ag film and a HNAF is illuminated by visible light (Figure 4b), the optically thick smooth Ag film appears dark black while the HNAF displays a green color, which is visible to the naked eyes, as well as a well-defined boundary. This result means that a continuous thick film of HNAF allows appreciable light transmission at certain wavelengths. In addition, this sample also demonstrates that the HNAF can be fabricated over a large macroscopic area thanks to the feature of CL. Moreover, HNAF islands with a random borderline are fabricated in the Ag film with the same thickness (100 nm), showing different apparent optical transmission comparing the two different films (Figure 4c). This result illuminates the great potential for resonant optical transmission to be used in pattern displays. In addition, the spectra and colors are the same no matter if the white light vertically illuminates from the hole side or the tip side. The property of greatly enhanced optical transmission at certain wavelengths offers more opportunities for thick metal films (without holes) in related applications.

In this metallic nanostructure, light scattering might occur and create light propagation paths along many directions. However, in this case the light also experiences the corresponding intensity changes. If scattering would be the main reason for the enhanced optical transmission, light at all wavelengths would pass through the film, and the colors would not be the same for samples illuminated from the hole side or the tip side with the different surface morphologies. This is not in agreement with the experimental results. Furthermore, extraordinary optical transmissions with well-defined maxima and minima are observed through 150, 200, and 300 nm (the actual film thickness on the side of the nanocones is higher than 100 nm) HNAF (Supporting Information Figure S2), proving again that optical scattering is not dominant. Hence these analyses and experimental results imply that more specific reasons should be responsible for the anomalous optical transmission. SPRs—collective excitations of surface electrons induced by light—are considered to be responsible for this.

The great enhancement in light transmission is predicted to arise from the improved SPR excited by the unique structural features, and this is described in Figure 4d. The solid nanocone array film of previous work with the same main structural parameters as the HNAF has nearly zero transmission in the visible range, which is very similar to the smooth Ag film (Supporting Information Figure S3). The novelty of the HNAF here is the hollow-core construction, lending the HNAF the two salient structural features of sharp top tips and bottom nanoholes. For this unique hollow cone-on-hole structure the following most simple and easily understandable explanations of the specific optical transmission can be given: According to previous analysis and experimental results, strong SPRs could be excited around the holes and along the film,[18,19] resulting in extraordinary optical transmission (EOT).[25] Moreover, the sharp nanocone tips are the pronounced places where the SP energy is focused, making the electric field intensity of nanocones much stronger than that of other nanostructures.[21,22] If then the two types of nanostructures, both possessing strong SPRs, are established in one HNAF, interactions of these strong SPRs are expected to greatly enhance the intensity of the SP field, which accounts for the intriguing optical transmission through the thick topologically continuous films.

To further understand and quantify the origin of this phenomenon, finite-difference time-domain (FDTD) simulations of spectra and distribution of the normalized electric field intensity ($|E|^2/|E_0|^2$) have been performed as shown in Figure 5 for the nanohole array (an Ag coating with circular holes), hollow-cone array (separated Ag hollow cones), and HNAF. The simulated structures are described in the inset images in Figure 5a, e, and i for the same corresponding main structural parameters of these nanostructures. The simulated distributions of $|E|^2/|E_0|^2$ are given at peak

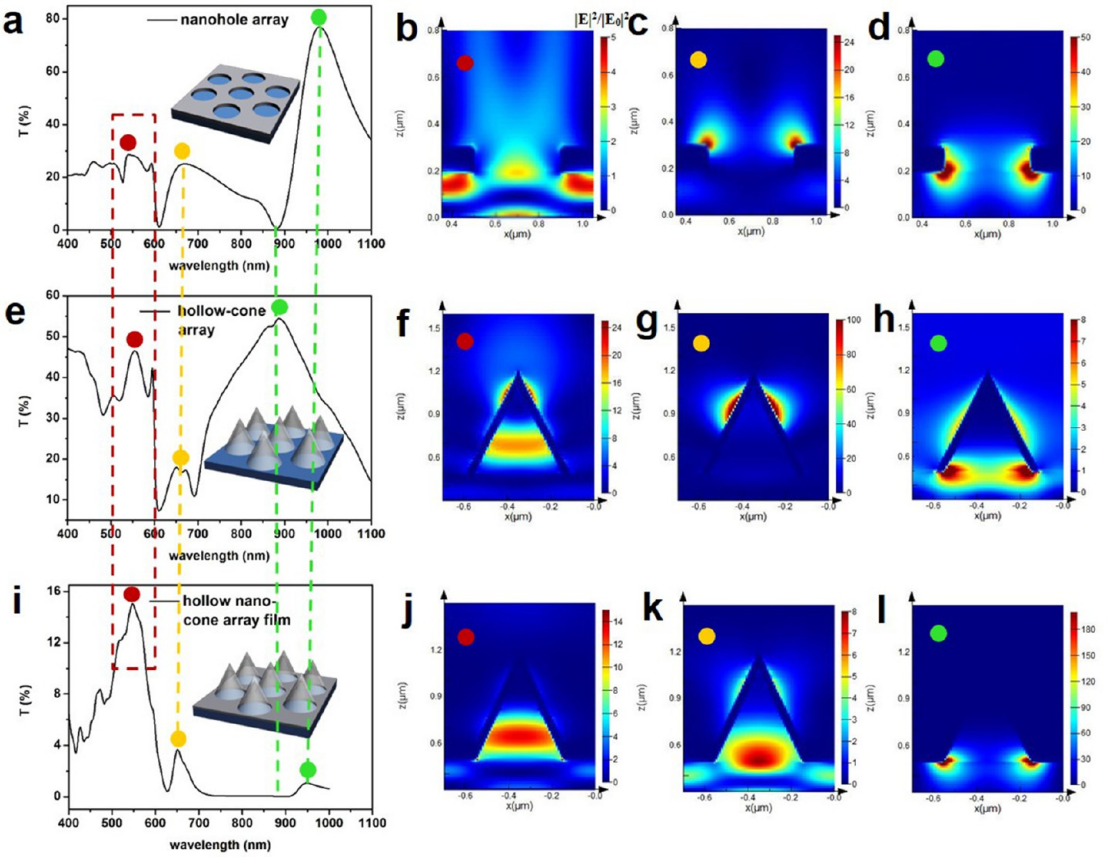

Figure 5. (a) Calculated transmission spectrum of the nanohole array. Simulated distributions of normalized electric field intensity at the peak wavelengths indicated by the (b) red, (c) yellow, and (d) green dots in (a). (e) Calculated transmission spectrum of hollow-cone array. Simulated distributions of normalized electric field intensity at the peak wavelengths indicated by the (f) red, (g) yellow, and (h) green dots in (e). (i) Calculated transmission spectrum of the HNAF. Simulated distributions of normalized electric field intensity at the peak wavelength indicated by (j) red, (k) yellow, and (l) green dots in (i). The red dotted frame and blue and green dotted lines in (a), (e), and (i) indicate the overlap of the transmission peaks. The gray and blue parts of the inset images in (a), (e), and (i) represent the materials of Ag and glass substrate, respectively.

wavelengths indicated by the red, yellow, and green dots in the corresponding calculated spectrum. For the simulated transmission spectra of the nanohole array in Figure 5a, the peaks indicated by the red, yellow, and green dots are assigned as the (1, 1), (1, 0) Ag/air transmission peaks, and (1, 0) Ag/glass transmission peak according to previous theoretical calculations.[26] The SP energy at the three peak wavelengths is mainly located in the center of the nanohole and the Ag/glass interface, Ag/air interface, and the Ag/glass interface, as shown in Figure 5b–d, confirming the above assignments. Figure 5e shows the calculated spectrum of the hollow-cone array, which also displays three main peaks. It can be seen in Figure 5f that the electric fields at the peak wavelength indicated by the red dot are distributed in regions around the tip and in the hollow core. The other two peaks are generated by the SP energy excited around the tip and at the glass/Ag interface, which are respectively shown in Figure 5g and Figure 5h.

The calculated spectrum of the HNAF in Figure 5i shows a main transmission peak and two much weaker peaks. The three peaks are indicated by red, yellow, and green dots, respectively. The simulated optical transmission of the main peak is more than 300 times that of a smooth film with the same average thickness (Supporting Information S3a). Furthermore, this value of transmission is more than 3 times higher than the theoretical result for the same thick film with ridge gratings.[5] Compared with the transmission spectra in Figure 5a and Figure 5e, it is observed that the transmission spectrum of the HNAF is well fitted by the overlap between the transmission spectra of the nanohole array and the hollow-cone array, which is indicated by the red dotted frame and yellow and green dotted lines, respectively. The result demonstrates that the transmission peaks of the HNAF are generated by the coupling of the nanohole array base and the upper hollow-cone caps. Moreover according to the simulated distributions of SP energy, the electric fields of the three peaks that experience the maxima are mainly distributed in regions in the hollow core of the nanocone (Figure 5j), around the tip and air/glass interface (Figure 5k), and limited at the Ag/glass interface

(Figure 5l). These redistributions of SP energy also fit well to the expected results of the interaction of SPRs excited by the nanohole base and nanocone caps. Therefore a convincing explanation for the greatly enhanced transmission is that the hollow cone and nanohole could support partially localized SPRs (LSPRs), and as the propagating surface plasmon polariton (SPP) is excited along the film, the contributions of both the LSPRs and SPP lead to redistribution and enhancement in electric field, resulting in this intriguing phenomenon.

For the redistribution of SP energy, the most prominent part is that of the main peak. Because both the hollow cone and nanohole have strong SPRs located in air at the wavelengths indicated by the red dots (Figure 5b and Figure 5f), the interaction between them causes a redistribution of the SP energy of the HNAF in air and a much stronger localization and enhancement outside the dielectric substrate. This fact is responsible for the strong transmission peak at ~540 nm. Furthermore, the field enhancement is not exclusively confined to the Ag surfaces as it is for the planar solid films, which greatly suppresses the substrate effect. This result is very advantageous for the sensing performance of the HNAF according to previous analysis,[27] and we will study this in subsequent work. For the peaks indicated by the yellow and green dots, the specific distribution of SP energy of the nanoholes (Figure 5c, Figure 5d) and hollow cones (Figure 5g, Figure 5h) causes either a much smaller enhancement of the electric fields derived from their coupling (Figure 5k) or a confinement to a smaller area (Figure 5l) than that in Figure 5j. Then the peaks resulting from the electric fields in Figure 5k and Figure 5l are emerging as two much weaker ones.

A deeper physical view can be developed based on the above analyses and the SPR process if the HNAFs are considered to be similar to nanohole arrays. When a sample is illuminated from one side, a plasmon is excited on this side due to the periodicity of the nanostructures. This is the same for the HNAFs and nanohole arrays. However, for nanohole arrays, the plasmon would be transferred to the other side through "optical tunneling" *via* the apertures, which is realized by the strong LSPR on the edge of the apertures. In contrast in this work the HNAFs are thick and continuous (without holes), which would prevent the transfer of the plasmon. Actually, the plasmon experiences a nearly complete attenuation for the flat metal film and solid nanocone arrays, eliminating the transmission (Supporting Information Figure S3). But for the HNAF, greatly enhanced LSPR can be excited in the hollow core due to the composite cone-on-hole structure (Figure 5j). The SP energy can be so strong that the plasmon on the illuminated side would tunnel through the thick continuous metal film to the other side although without apertures. This plasmon, in turn, radiates the energy to the far-field. This view is in accord with previous findings that the presence of holes is not necessary for the extraordinary optical transmission, but they provide a lower attenuation than continuous metal films.[5] This conclusion is also confirmed by the fact that the optical performances of HNAFs are the same for the samples illuminated from the hole side or the tip side. The independence from the illumination direction is the same as the feature of the EOT effects and also indicates that the plasmon on both sides is a superposition, showing the possibility of plasmon transfer. Overall, much more effective SP excitations based on the cone-on-hole nanostructure enable plasmon transfer to the opposite side, leading to the greatly enhanced optical transmission.

Figure 6a and b show the measured and calculated transmission spectra of the corresponding HNAFs in Figure 2 and Figure 3, which can be directly compared. The overall qualitative agreement between experimental and simulated profiles is good, and the remaining discrepancy can be attributed to extra losses in the metal due to increased surface scattering, the rough Ag surface, and the inhomogeneity of the inter-nanocone separation. The main transmission peak shows a blue-shift and a reduction in transmission intensity with a decrease of height and diameter. In addition, the transmission peaks of hollow nanocones with heights/diameters of 300/300 nm and 200/280 nm cannot be recognized due to the low transmission, and the optical transmission becomes similar to that of the planar Ag film. According to previous reports,[28] the peak position is hardly affected by the hole diameter, which can be neglected relative to the effect of the heights. Therefore the peak positions are mainly determined by the heights, which can be demonstrated by means of the SP energy distributions (Figure 6c−e). It is noted that comparing the simulations of hollow nanocone arrays with reduced heights demonstrates apparent differences in energy density and location. As the distance between the tips and holes is decreased, the interactions are getting stronger, leading to the blue-shift of the main peaks in Figure 6b. However, the maximum of the SP energy is drawn near the substrate, as the height decreases and the condition of SPR is more similar to that of 2D nanohole arrays. This brings about the reduction in transmission intensity.

In summary, although a metal film of 100 nm thickness is optically thick, coupling of light with the HNAF is greatly improved based on the unique hollow feature, enabling the realization of greatly enhanced optical transmission through thick metal films. On the basis of the resonant optical transmission, the hollow nanocone array films can be used as advanced materials for microreactors making use of the local field intensity, which may be increased up to an order of magnitude for photoinduced reactions and monitoring, isolated cell culture bases, *etc*., which are difficult to realize for

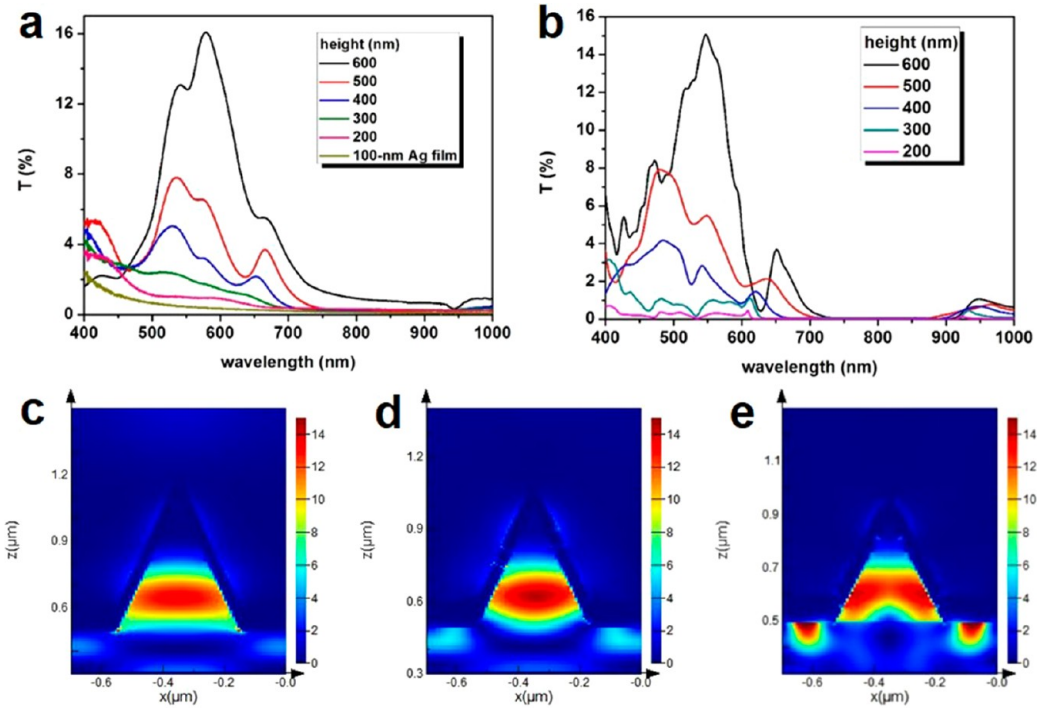

Figure 6. (a) Measured and (b) calculated transmission spectra of HNAFs with heights/diameters of 600/400 nm, 500/350 nm, 400/320 nm, 300/300 nm, and 200/280 nm. The transmission spectrum of a 100 nm planar Ag film is also shown in (a). Normalized near-field electric field profile ($|E|^2/|E_0|^2$) simulated at the main peak wavelengths of hollow nanocone arrays with heights of (c) 600 nm, (d) 500 nm, and (e) 400 nm.

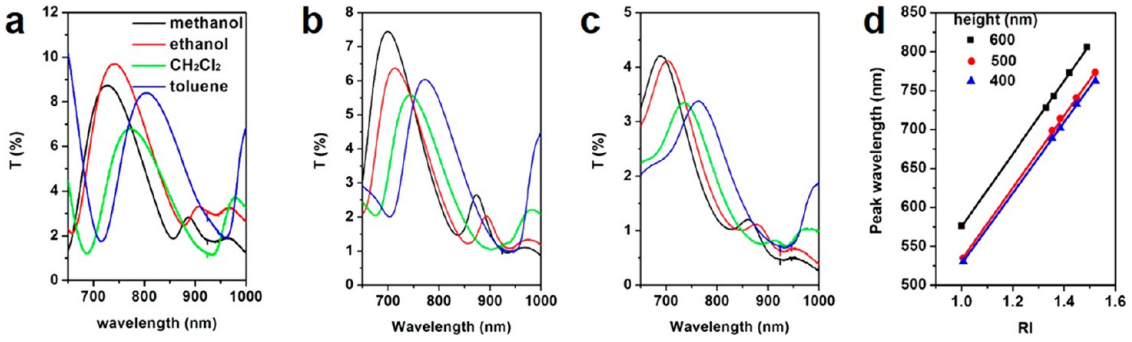

Figure 7. Transmission spectra of hollow nanocone arrays with heights of (a) 600 nm, (b) 500 nm, and (c) 400 nm measured by immersing samples in a sequence of liquids with increasing RI: methanol (1.33), ethanol (1.36), dichloromethane (1.42), and toluene (1.49). (d) Linear fit for the hollow nanocone arrays with heights of 600 nm (square symbols, R^2 = 0.99956), 500 nm (circular symbols, R^2 = 0.99890), and 400 nm (triangular symbols, R^2 = 0.99931).

thin films or perforated films. This provides a high potential due to the combination of high optical sensitivity and chemistry in microcavities.

Performance of Hollow Nanocone Array Films in Sensing. For testing the performance in sensing, hollow nanocones with heights of 600, 500, and 400 nm were immersed in a sequence of liquids with increasing refractive index (RI), and the transmission spectra were measured as shown in Figure 7. Moreover, the performance of hollow nanocone arrays with lower heights cannot be investigated because of unidentified peaks. Significant red-shifts of the peaks are observed in Figure 7a–c, which further shows different sensitivities. Figure 7d shows linear fits of the main transmission peaks in air as a function of solution refractive index. Strictly linear responses are observed for all three samples, which cannot be achieved for conventional nanohole arrays. The sensitivities indicated by the slope of the lines are measured as shown in Table 1, in which the hollow nanocone array with 500 nm height possesses the highest sensitivity. Moreover, the values are much higher than those of ordered two-dimensional (2D) nanohole arrays fabricated in a previous report (400 nm/RIU),[29] random 2D nanoholes (71–270 nm/RIU),[30,31] and nanoparticles and 2D nanoparticle arrays (76–200 nm/RIU).[32,33]

To express the sensitivity in a way equally appropriate for different morphologies and parameters of metallic nanostructures with resonances in the spectral range from visible to infrared, the relative RIS is

TABLE 1. Sensitivity and Relative RIS of Hollow Nanocone Arrays with Different Heights

sample	height (nm)	sensitivity (nm/RIU)[a]	RIS_{relat} (RIU^{-1})
1	600	467	59%
2	500	486	64%
3	400	478	63%

[a] nm per refractive index unit.

introduced as reported by Shumaker-Parry and coworkers.[12] The relative RIS is the ratio of sensitivity in eV/RIU to the light energy in eV at the resonance wavelength multiplied by 100% and is defined by the following equation:

$$\mathrm{RIS}_{\mathrm{relat}} = \frac{1}{\omega_r} \times \frac{\Delta\omega(\mathrm{eV})}{\Delta n} \times 100\% \qquad (1)$$

ω_r is the resonance energy with units of eV, and $\Delta\omega/\Delta n$ is the bulk RIS with units of eV/RIU. The relative sensitivity of hollow nanoncone arrays, calculated as shown in Table 1, is higher than the highest relative sensitivity of 38%/RIU measured for crescents,[12] the highest value of 40%/RIU for hematite-gold core–shells or rices,[34] and the highest relative sensitivity of 61%/RIU for films perforated with nanoholes.[35] In particular, the hollow nanocone arrays with a height of 500 nm show the highest relative sensitivity.

The enhanced performances of robust linear responses and distinctions among the samples with different heights can be demonstrated by means of the SP energy distributions in Figure 6. The SP energy of the hollow nanoncone arrays is mainly located in air, resulting from the interactions of cone caps and nanohole array foundations. The results indicate the existence of a more localized and enhanced SP field outside the dielectric substrate (in the hollow core) and the full accessibility to the field enhancement region for species to be detected, which can explain the boost in sensitivity and excellent linear fitting. Simulated results indicate that liquids could enter into the hollow core due to capillarity forces (Supporting Information Figure S4). Besides, the sensing performance is considered to be the result of liquid on one side of the attached part but on both sides of the convex nanostructure (hollow nanocones) according to the simulation results in Supporting Information Figure S4. This unique feature of accessibility to detected species from both sides of the hollow nanocones is also the exact reason for the enhancement in sensing performance. As the distance between the tips and holes is reduced, the interactions are getting stronger, resulting in higher sensitivity for the sample with 600 nm height than that of the one with 500 nm height. However, due to the smaller distance, SP energy of the one with 400 nm height is more affected by the substrate, which causes a lower sensitivity than that of hollow nanocone arrays with 500 nm height. Therefore, the sample with a height of 500 nm is most appropriate and shows the highest sensing performance.

CONCLUSIONS

In summary, films with hollow nanocone arrays can be fabricated by a simple and efficient colloidal lithography method. The method is versatile and inexpensive and can be applied with only little sophisticated equipment. The topologically continuous films show greatly enhanced optical transmission with well-defined maxima and minima. Moreover, the optical measurements indicate a promising type of structural films with novel SP effects due to the specific hollow elements. FDTD simulations demonstrate that the enhanced transmission is generated by the greatly enhanced plasmon excitation and further determined by the height of nanocones and thickness of the films. Calculations show good agreement with the measured spectra. Moreover, the topologically continuous films are highly sensitive to the surrounding environment with a strictly linear and strong dependence on refractive index, showing great potential for plasmonic sensors. The use of this novel type of continuous film is promising for advanced optical applications that are difficult to realize by thin films or films with holes. For applications as microreactors and as versatile substrates for analysis of single molecules, cell cultures, *etc.*, special use can be made of the fact that the plasmon field is enhanced near the pronounced structural elements in a predictable way, enabling the monitoring of chemical or biological processes near these elements and also initiating these reactions. Furthermore, the results in this paper demonstrate that micro-nanostructures may provide characteristics to certain materials that would not have been directly derived from those of the components. They can change the fundamental properties based on specific structures, especially the optical properties and their dependence on the environment, enabling a plethora of new applications.

METHODS

Materials. In all experiments deionized water was ultrapure (18.2 MΩ·cm) from a Millipore water purification system. The glass slides (15 × 30 mm^2) used as substrates were cleaned in an O_2 plasma cleaner for 2 min to create a hydrophilic surface. PS spheres of 700 nm were obtained from Wuhan Tech Co., Ltd. Photoresist (BP212-37 positive photoresist) was purchased from Kempur (Beijing) Microelectronics, Inc. The silver (99.9%) powder for vapor deposition was purchased from Sinopharm Chemical Reagent Co. Ltd. Methanol, ethanol, dichloromethane, and toluene were purchased from Beijing Chemical Works and were used as received.

Fabrication of Hollow Nanocone Array Films. Photoresist was spin-coated onto the glass substrate and cured at 88 °C for 2 h. Next the PS sphere (700 nm) monolayers were prepared on the as-prepared substrate by the interface method.[23] Oxygen reactive ion etching, performed on a Plasmalab Oxford 80 Plus system (ICP 65) (Oxford Instrument Co., UK), was applied for 240, 270, 300, 330, and 360 s, eliminating the PS spheres and generating cones with heights of 600, 500, 400, 300, and 200 nm. The RIE procedure was performed at a pressure of 10 mTorr, a flow rate of 50 sccm, a radio frequency power of 100 W, and an inductively coupled plasma (ICP) power of 200 W. After that the samples were mounted in a thermal evaporator to vertically deposit 100, 150, 200, and 300 nm of Ag (99.9%), respectively. Finally the photoresist was washed away by ethanol. After these procedures, the hollow nanocone array film was formed.

Finite-Difference Time-Domain Simulations. A commercial software package (FDTD Solutions v8.6.3, Lumerical Solutions Inc.) was used to perform simulations of electromagnetic fields with the same structural parameters as extracted from the actual fabricated samples. The structure was excited by a normally incident, unit magnitude plane wave propagating in the *z* direction with an electric field polarization along the *x*-axis. A rectangular unit cell consisting of one hollow cone in the center and four quartering cones at the four corners was used with periodic boundary conditions in two dimensions to simulate an infinite array of periodic hollow nanocones, and perfectly matched layer boundary conditions were used on the top and bottom surfaces of the simulation domain to simulate the infinite volumes of the air and the silicon material, respectively. The auto nonuniform mesh was chosen in the entire simulation domain for higher numerical accuracy, while the time step $\Delta t \approx 2.73 \times 10^{-17}$ s was chosen to satisfy the Courant stability condition. The mesh refinement is the conformal variant 2. Monitors of frequency-domain field profile and frequency-domain field and power were placed to calculate the distributions of SP energy and the transmission spectra in the continuous wave normalization state. The magnitude of the incident electric fields was taken to be unity, and the enhancement of electromagnetic fields evaluated. The optical parameters of Ag and SiO_2 were taken from Palik's handbook.

Characterization. Scanning electron microscopy images were taken with a JEOL JSM 6700F field emission scanning electron microscope with a primary electron energy of 3 kV, and the samples were sputtered with a layer of Pt (*ca.* 2 nm thick) prior to imaging to improve conductivity. Height analyses were taken under tapping mode with a Nanoscope IIIa scanning probe microscope from Digital Instruments under ambient conditions. A Maya 2000PRO optics spectrometer and a model DT 1000 CE remote UV/vis light source (Ocean Optics) were used to measure the transmission spectra.

Conflict of Interest: The authors declare no competing financial interest.

Acknowledgment. This work was supported by the National Natural Science Foundation of China (51073070, 51173068, 51373066).

Supporting Information Available: SEM images of etching processes with different durations; transmission spectra of 150, 200, and 300 nm hollow nanocone array films; simulated transmission spectra of a smooth 100 nm Ag film and a solid nanocone array film; simulated transmission spectra of hollow nanocone array films with a height of 600 nm immersed in ethanol with different conditions. This material is available free of charge via the Internet at http://pubs.acs.org.

REFERENCES AND NOTES

1. Gordon, J. G.; Ernst, S. Surface Plasmons as a Probe of the Electrochemical Interface. *Surf. Sci.* **1980**, *101*, 499–506.
2. Sarid, D. Long-Range Surface-Plasma Waves on Very Thin Metal Films. *Phys. Rev. Lett.* **1981**, *47*, 1927–1930.
3. Gu, Z.; Dummer, R. S.; Maradudin, A. A.; McGurn, A. R.; Mendez, E. R. Enhanced Transmission through Rough-Metal Surfaces. *Appl. Opt.* **1991**, *30*, 4094–4102.
4. Homola, J. Surface Plasmon Resonance Sensors for Detection of Chemical and Biological Species. *Chem. Rev.* **2008**, *108*, 462–493.
5. Bonod, N.; Enoch, S.; Li, L.; Popov, E.; Nevière, M. Resonant Optical Transmission through Thin Metallic Films with and without Holes. *Opt. Express* **2003**, *11*, 482–490.
6. Gérard, D.; Salomon, L.; de Fornel, F.; Zayats, A. V. Ridge-Enhanced Optical Transmission through a Continuous Metal Film. *Phys. Rev. B* **2004**, *69*, 113405.
7. Okamoto, T.; Simonen, J.; Kawata, S. Plasmonic Band Gaps of Structured Metallic Thin Films Evaluated for a Surface Plasmon Laser Using the Coupled-Wave Approach. *Phys. Rev. B* **2008**, *77*, 115425.
8. Altewischer, E.; Genet, C.; van Exter, M. P.; Woerdman, J. P.; Alkemade, P. F. A.; van Zuuk, A.; van der Drift, E. W. J. M. Polarization Tomography of Metallic Nanohole Arrays. *Opt. Lett.* **2005**, *30*, 90–92.
9. Ohno, T.; Bain, J. A.; Schlesinger, T. E. Observation of Geometrical Resonance in Optical Throughput of Very Small Aperture Lasers Associated with Surface Plasmons. *J. Appl. Phys.* **2007**, *101*, 083107.
10. Shumaker-Parry, J. S.; Rochholz, H.; Kreiter, M. Fabrication of Crescent-Shaped Optical Antennas. *Adv. Mater.* **2005**, *17*, 2131–2134.
11. Zhu, F. Q.; Fan, D. L.; Zhu, X. C.; Zhu, J. G.; Cammarata, R. C.; Chien, C. L. Ultrahigh-Density Arrays of Ferromagnetic Nanorings on Macroscopic Areas. *Adv. Mater.* **2004**, *16*, 2155–2159.
12. Bukasov, R.; Shumaker-Parry, J. S. Highly Tunable Infrared Extinction Properties of Gold Nanocrescents. *Nano Lett.* **2007**, *7*, 1113–1118.
13. Fredriksson, H.; Alaverdyan, Y.; Dmitriev, A.; Langhammer, C.; Sutherland, D. S.; Zaech, M.; Kasemo, B. Hole–Mask Colloidal Lithography. *Adv. Mater.* **2007**, *19*, 4297–4302.
14. Prikulis, J.; Hanarp, P.; Olofsson, L.; Sutherland, D.; Kall, M. Optical Spectroscopy of Nanometric Holes in Thin Gold Films. *Nano Lett.* **2004**, *4*, 1003–1007.
15. Zhang, G.; Wang, D. Fabrication of Heterogeneous Binary Arrays of Nanoparticles *via* Colloidal Lithography. *J. Am. Chem. Soc.* **2008**, *130*, 5616–5617.
16. Zhang, G.; Wang, D.; Möhwald, H. Fabrication of Multiplex Quasi-Three-Dimensional Grids of One-Dimensional Nanostructures *via* Stepwise Colloidal Lithography. *Nano Lett.* **2007**, *7*, 3410–3413.
17. Zhang, G.; Wang, D. Colloidal Lithography—the Art of Nanochemical Patterning. *Chem.—Asian J.* **2009**, *4*, 236–245.
18. Krishnan, A.; Thio, T.; Kim, T. J.; Lezec, H. J.; Ebbesen, T. W.; Wolff, P. A.; Pendry, J.; Martin-Moreno, L.; Garcia-Vidal, F. J. Evanescently Coupled Resonance in Surface Plasmon Enhanced Transmission. *Opt. Commun.* **2001**, *200*, 1–7.
19. Ai, B.; Yu, Y.; Möhwald, H.; Zhang, G. Novel 3D Au Nanohole Arrays with Outstanding Optical Properties. *Nanotechnology* **2013**, *24*, 035303.
20. Ai, B.; Yu, Y.; Möhwald, H.; Zhang, G. Responsive Monochromatic Color Display Based on Nanovolcano Arrays. *Adv. Opt. Mater.* **2013**, *1*, 724–731.
21. Martín-Cano, D.; Martín-Moreno, L.; García-Vidal, F. J.; Moreno, E. Resonance Energy Transfer and Superradiance Mediated by Plasmonic Nanowaveguides. *Nano Lett.* **2010**, *10*, 3129–3134.
22. Chen, Y.; Cruz-Chu, E. R.; Woodard, J. C.; Gartia, M. R.; Schulten, K.; Liu, L. Electrically Induced Conformational Change of Peptides on Metallic Nanosurfaces. *ACS Nano* **2012**, *6*, 8847–8856.
23. Rybczynski, J.; Ebels, U.; Giersig, M. Large-Scale, 2D Arrays of Magnetic Nanoparticles. *Colloids Surf. A* **2003**, *219*, 1–6.
24. Tan, W.-C.; Preist, T. W.; Sambles, R. J. Resonant Tunneling of Light through Thin Metal Films *via* Strongly Localized Surface Plasmons. *Phys. Rev. B* **2010**, *62*, 11134.
25. Ebbesen, T. W.; Lezec, H. J.; Ghaemi, H. F.; Thio, T.; Wolff, P. A. Extraordinary Optical Transmission through Sub-Wavelength Hole Arrays. *Nature* **1998**, *391*, 667–669.
26. Van der Molen, K. L.; Segerink, F. B.; Van Hulst, N. F.; Kuipers, L. Influence of Hole Size on the Extraordinary Transmission through Subwavelength Hole Arrays. *Appl. Phys. Lett.* **2004**, *85*, 4316–4318.

27. Dmitriev, A.; Hägglund, C.; Chen, S.; Fredriksson, H.; Pakizeh, T.; Käll, M.; Sutherland, D. S. Enhanced Nanoplasmonic Optical Sensors with Reduced Substrate Effect. *Nano Lett.* **2008**, *8*, 3893–3898.
28. Laux, E.; Genet, C.; Ebbesen, T. W. Enhanced Optical Transmission at the Cutoff Transition. *Opt. Express* **2009**, *17*, 6920–6930.
29. Brolo, A. G.; Gordon, R.; Leathem, B.; Kavanagh, K. L. Surface Plasmon Sensor Based on the Enhanced Light Transmission through Arrays of Nanoholes in Gold Films. *Langmuir* **2004**, *20*, 4813–4815.
30. Dahlin, A.; Zäch, M.; Rindzevicius, T.; Kall, M.; Sutherland, D. S.; Höök, F. Localized Surface Plasmon Resonance Sensing of Lipid-Membrane-Mediated Biorecognition Events. *J. Am. Chem. Soc.* **2005**, *127*, 5043–5048.
31. Rindzevicius, T.; Alaverdyan, Y.; Dahlin, A.; Höök, F.; Sutherland, D. S.; Käll, M. Plasmonic Sensing Characteristics of Single Nanometric Holes. *Nano Lett.* **2005**, *5*, 2335–2339.
32. Nath, N.; Chilkoti, A. A Colorimetric Gold Nanoparticle Sensor to Interrogate Biomolecular Interactions in Real Time on a Surface. *Anal. Chem.* **2002**, *74*, 504–509.
33. Hartlen, K. D.; Athanasopoulos, A. P. T.; Kitaev, V. Facile Preparation of Highly Monodisperse Small Silica Spheres (15 to >200 nm) Suitable for Colloidal Templating and Formation of Ordered Arrays. *Langmuir* **2008**, *24*, 1714–1720.
34. Wang, H.; Brandl, D. W.; Le, F.; Nordlander, P.; Halas, N. J. Nanorice: a Hybrid Plasmonic Nanostructure. *Nano Lett.* **2006**, *6*, 827–832.
35. Li, Y.; Pan, J.; Zhan, P.; Zhu, S.; Ming, N.; Wang, Z.; Han, W.; Jiang, X.; Zi, J. Surface Plasmon Coupling Enhanced Dielectric Environment Sensitivity in a Quasi-Three-Dimensional Metallic Nanohole Array. *Opt. Express* **2010**, *18*, 3546–3555.